JOURNAL OF MATERIALS SCIENCE 22 (1987) 4251–4266

Deformation and fracture behaviour of niobium–10 at % vanadium alloy with hydrogen

K. JAGANNADHAM
Materials Science and Engineering, North Carolina State University, Raleigh, North Carolina 27695-7916, USA

The results of a systematic study of deformation and fracture behaviour of niobium–10 at % vanadium alloy with or without a nominal 200 p.p.m. wt % hydrogen and deformed in tension are presented as function of orientation and two testing temperatures; 195 and 295 K. Single crystals, large and small grain size polycrystals are used to determine the mechanisms of hydrogen embrittlement. Metallographic observations using both optical and scanning electron microscopy of the surface features associated with deformation and fracture behaviour of this alloy containing hydrogen are illustrated. In particular, the relationship between slip, twinning and cracks is described. Furthermore, the reasons for the relatively large ductility associated with niobium rich alloys in comparison with other Nb–V alloys are put forward. Discrete dislocation analysis of the models of twinning is used to substantiate the ideas presented on the effect of hydrogen on the nucleation of twins and cracks in this alloy.

1. Introduction

The mechanical behaviour of body centred cubic refractory alloys, in particular of the niobium–vanadium system, has been studied extensively as these alloys can be easily fabricated and also possess desirable mechanical properties [1–10]. In addition, the tendency for embrittlement in the presence of hydrogen in these alloys, coupled with high hydrogen solubility has aroused considerable interest. Many interesting experimental results are obtained which illustrate the effect of hydrogen on the mechanical properties of polycrystalline niobium–vanadium alloys [4–10]. However, there has been no systematic study using single crystals of Nb–V alloy in a manner similar to the results obtained in niobium single crystals [11–24]. In particular, while the tendency for embrittlement is very high for alloys of various compositions of niobium–vanadium system, niobium rich alloys containing vanadium over a smaller percentage range offer better resistance [10] in the presence of hydrogen.

Barring the situation of anomalous slip observed in ultra-high purity single crystals with the tensile axis oriented close to 0 0 1 pole [14–17], the crystallographic nature of slip in niobium may be summarized [11–17] by stating that above liquid nitrogen temperatures, slip confines to the highly stressed (1 1 2) type planes for orientations close to 0 0 1; to the (1 0 1) type planes for centre triangle orientations and to the (2 1 1) or (3 1 2) type planes for orientations close to the 0 1 1–$\bar{1}$ 1 1 boundary. However, at lower temperatures, as a result of twinning–antitwinning asymmetry [18], deformation twinning becomes favoured for orientations close to 0 0 1 in tension and for orientations near the 0 1 1–$\bar{1}$ 1 1 boundary in compression, with the operating twinning system being the most highly stressed.

In the past, it has been shown that twinning is a common feature of deformation in many niobium–vanadium alloys in the polycrystalline form subjected to tension at lower temperatures [6–10]. On the other hand, twinning is conspicuously absent in niobium-rich vanadium alloys at the same temperatures. Further, it is also argued that irradiation defects and elements such as oxygen and nitrogen that occupy interstitial positions suppress twinning [9, 25] while the presence of hydrogen increases the tendency for twinning [26, 27] as noted from the increase in the temperature at which twinning is observed.

This paper presents results of mechanical tests carried out in tension at two different temperatures (295 and 195 K) on single crystals and large grain size polycrystals of niobium rich vanadium alloys (8–10 at % vanadium) with high hydrogen solid solubility. This is the first systematic study of deformation and fracture behaviour exhibited by a hydrogen-embrittled niobium–vanadium alloy under tension as a function of orientation of the crystal and also attempts to provide the reasons for the higher ductility exhibited by the niobium-rich alloys in the presence of hydrogen. Also, it becomes possible to determine whether hydrogen introduces twinning, either by increasing the frictional stress to slip or by increasing the tendency for nucleation of cleavage cracks which inturn produce stress concentration high enough for twinning to take place. The results of a few tensile tests carried out on polycrystalline small grain size samples charged with different weight percentages of hydrogen are also presented. The presence of intergranular fracture in this alloy with hydrogen in solid solution is discussed in the light of these results. Since grain boundary cracks are easily nucleated in higher vanadium alloys in the presence of hydrogen [10], it becomes possible to propose a unifying idea on the

0022–2461/87 $03.00 + .12

weakening of grain boundaries as a result of distortion introduced by trapping of hydrogen near vanadium atoms.

2. Experimental procedure

Niobium and vanadium (5.74 wt %) of the electron beam melted purity were combined by arc melting in an argon atmosphere to make a niobium–10 at % vanadium alloy. Several attempts were made to make a single crystal of this alloy by the electron beam float zone technique. However, invariably most of the vanadium in the alloy is depleted in the vapour form due to high vapour pressure of vanadium at the melting point of this alloy [28]. Hitherto, other techniques such as strain annealing have been only partially successful and require further improvement. On the other hand, sufficiently large polycrystals with grain size as large as 1 cm × 0.5 cm × 0.5 cm have been produced by the following method. The alloy is placed in a water cooled copper boat and an arc is passed over it at a critical speed of approximately 1/4 inch h^{-1} in an argon atmosphere with a positive pressure maintained so that vanadium does not vapourize. The method being perfected in the present stage depends in an unknown manner on several parameters involved, such as speed at which the arc is moved, depth of the copper boat or the thickness of the alloy bulk being melted and power input into the system. However, it is believed that the very high temperature gradient between the molten alloy at the top and the water cooled copper boat at the bottom provides the driving force for the large grain growth observed. The positive pressure of argon atmosphere maintained during melting as well as during production of large grain size material was found to limit vanadium loss to no more than 1 wt %.

A very important aspect of making crystals of this alloy is that the formation of microscopic cavities could not be prevented completely. Through several attempts to eliminate the formation of cavities in the alloy, it was found that the difference in the density of the melt and the solid phase was responsible for formation of microscopic cavities [29]. Slices of the alloy, cut from large grain size bulk were used to make specimens which could be pin loaded in tension. Scanning electron microscopic examinations did not show the presence of any cavities on the fracture surfaces of this alloy. In order to avoid the possibility of failure of the specimens near the pin holes during testing, deformation was introduced in the grip region of the specimens by compression. Subsequently, the surfaces were ground to 600 grit and the specimens electropolished in 6 vol % sulphuric acid in methanol at temperatures below − 50° C. Further, the specimens were annealed near 1300° C for 3 h to recrystallize and introduce a smaller grain size in the region of the grips so that when charged with hydrogen and loaded in tension, plastic deformation is confined to the gauge length. A few specimens with threaded ends and square milled cross-section in the gauge length were also made without altering the grain size in the grip region.

In order to analyse the crystallographic nature of a slip or a twin system and a crack plane, X-ray back reflection Laue pictures of two perpendicular surfaces were taken for each grain in the specimen and analysed to determine the exact angular rotation required to obtain the stereographic projection of orientation of one surface from that of the other. This enabled the subsequent two-surface trace analysis of the surface features so that slip, twin or crack plane could be determined without ambiguity [30, 31].

Hydrogen charging of the tensile specimens was started by preheating the samples to 1000° C under vacuum of 10^{-7} torr in a tube furnace and cooling it after 10 min to 850° C. The furnace was isolated from the external vacuum pump and opened to hydrogen generated from thermal decomposition of uranium hydride at a predetermined pressure. The samples were then maintained for nearly 3 h at 850° C in the hydrogen atmosphere and subsequently the power input to the furnace was shut off and the samples cooled to room temperature. A hydrogen concentration of nominally 200 p.p.m. wt was aimed for charging all specimens except in a few special ones. The samples were subsequently analysed at the end of tensile testing using chemical analysis for vanadium and vacuum fusion analysis for oxygen, nitrogen and hydrogen.

The quantity of oxygen by weight in all the specimens was found to be 170 ± 30 p.p.m., while that of nitrogen has been determined to be 40 ± 10 p.p.m. The concentration by weight of hydrogen was found to be 100 p.p.m. in Samples 1 to 4, 150 p.p.m. in Samples 5 to 8 and 180 p.p.m. in Samples 9 to 13. On the other hand, the wt % of vanadium in all samples was found to be near 4.5 ± 1.5%. A special mention of the analysis of Specimens 4, 6 and 8 is useful for subsequent discussion. In particular, Specimen 4 contained 73 p.p.m. hydrogen, 150 p.p.m. oxygen and 47 p.p.m. nitrogen; Specimen 6 contained 130 p.p.m. hydrogen, 200 p.p.m. oxygen and 43 p.p.m. nitrogen and Specimen 8 contained 185 p.p.m. hydrogen, 260 p.p.m. oxygen and 53 p.p.m. nitrogen, all by weight. Specimens 15 and 16 were not charged with hydrogen and hence no vacuum fusion analysis was carried out. A few specimens (2, 3, 13 and 14) were mechanically polished on 600 grit and further electrolytically polished below − 50° C in 6 vol % methanol containing sulphuric acid after charging with hydrogen at a nominal 200 p.p.m. wt %. These specimens were tested in tension to observe any difference in deformation and fracture behaviour that may have resulted due to the removal of excess hydrogen present in the vicinity of the surface.

Mechanical testing of the specimens was carried out on a screw driven floor model of an Instron machine at a cross-head speed of 0.005 inches min^{-1} or a strain rate of 0.83×10^{-4} sec^{-1} and the load–elongation curves were recorded on a chart. In order to minimize the effect of grain boundaries and the introduction of accommodation slip in adjacent grains, the specimens were deformed initially just above the yield point and unloaded for determination of the crystallographic nature of the deformation that took place well within the grains. It has been found that, except in a few

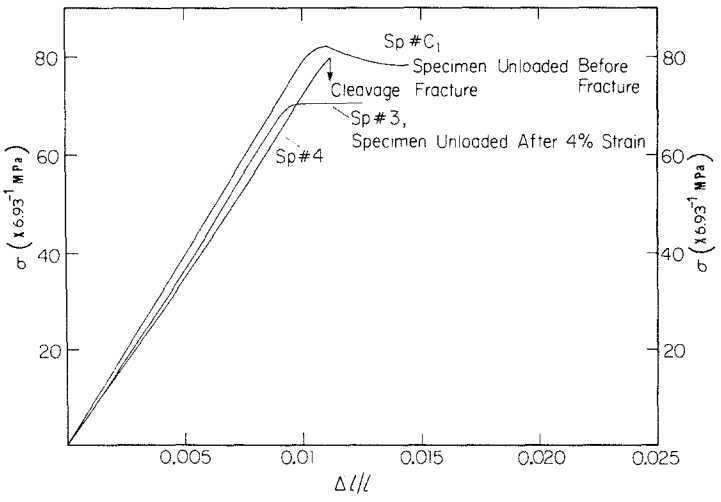

Figure 1 The stress against strain curves obtained for three typical specimens representative of all the other. Specimen 4 failed in a brittle manner, Specimen 3 elongated continuously with very little work hardening while Specimen C_1 has been unloaded after inferring the formation of a crack.

situations, slip has never been observed at the grain boundaries in this alloy, presumably because the grains were very large in size and hence very little constraint is exerted due to the neighbouring grains. Subsequently, the specimens were strained at the same strain rate as earlier until a return of the load–elongation curve or a sharp drop in the load was noticed from which the formation of a crack was inferred and latter further confirmed with metallographic observations. At times, the specimens failed without any noticeable deformation leading to an extreme brittle behaviour, as illustrated by the engineering stress against strain curves shown in Fig. 1.

The observation of slip lines, twins and cracks on the four perpendicular surfaces of the specimen was carried out using both optical microscopy in the DIC (differential interference contrast) method and scanning electron microscopy in the secondary electron emission method. Plastic deformation behaviour due to twinning was subsequently identified by electropolishing and chemically etching the specimens. In addition, the fracture surface on both faces of the crack has also been observed using the secondary electron emission method in order to characterize the fracture behaviour. The accuracy of the results plotted on a stereographic projection was only better than 5 to 6° due to several factors that limited gaining more accurate data. For example, the distortion of the surfaces due to plastic deformation, the rounding of the specimen edges during electropolishing, at times the wavy nature of the slip, to some extent the difficulty in orienting the surface of the grains perfectly normal to the X-ray beam and the charts which were not completely perfect for analysis, were the factors contributing to the afore mentioned limited accuracy of the results. At this point, it is useful to note that there is enough evidence in the literature to suggest that slip in bcc metals takes place on high index complex planes [19] and thus any deviation of the observed slip planes from the standard {1 1 0} or {1 1 2} type slip planes may not be a result of inaccuracy in the analysis.

The usefulness of employing large grain size specimens to determine the deformation and fracture behaviour of single crystals may be judged by the concurrence of the results obtained from several grains. The validity of the data was checked by testing several large grain size specimens and the results presented below are useful to prove that within a very small scatter, plastic deformation and fracture behaviour of all crystals as a function of orientation is consistent. In the past, other authors [32] have carried out similar experiments using large grain size specimens and obtained useful results on the twinning behaviour in bcc alloys.

3. Experimental observations

In this section, results of tests carried out on single crystals and large grain size polycrystals are mentioned first, followed by the results of those obtained from polycrystalline small grain size specimens. The nomenclature used in specifying the crystals and the grains should be followed carefully to determine the significance of the results presented in this paper. The first numeric indicates the specimen and the second used as a subscript describes the grain in which the observations were made. On the other hand, for cylindrical specimens, the specification starts with C followed by the first subscript to indicate the specimen number and the second to indicate the grain in which the observations were performed. In a few of the specimens, the subscript to indicate the grain is absent, namely 1, 3, 4, 6, 8, C_1, C_2 and C_3. Among these, specimens C_1, C_2 and C_3 are single crystals while 1, 3, 4, 6 and 8 are specimens wherein deformation and fracture within the gauge length is confined only to a single grain all the way up to fracture.

In order to verify the validity of Schmid's law [30] in this alloy, i.e. slip or twin system corresponds to those with maximum resolved shear stress, the Schmid's factor has been calculated and shown in Table I along with the Schmid–Boas number of the (1 1 2) type twinning plane [12]. The shear systems for which the Schmid's factor is the highest are listed along with the nature of the actually observed system. The letter (A) in parenthesis indicates the allowed twinning system and (F) the forbidden [12, 30]. It can be easily inferred from the results presented in Table I that provided the {1 1 0}, {1 1 2} and {3 1 2} are considered as the possible slip planes, plastic deformation by slip and twinning in this alloy follows Schmid's law. Among the few exceptions, the $(\bar{2}\,1\,1)[1\,1\,1]$ slip system is observed only when the orientation of the tensile axis is very close to or on the border connecting $\bar{1}\,1\,1$ and $0\,1\,1$ poles [18]. Similarly, the $(\bar{3}\,1\,2)[1\,1\,1]$ slip system could

TABLE I Schmid factors of the most highly stressed {1 1 2} and {1 1 0} type shear systems and their correlation with those actually observed. The temperature of the test was 195 K except in specimens 5 and 10. The forbidden twinning systems were not observed in all the crystals

Crystal (tensile axis)		System	Schmid factor	Schmid–Boas number	Nature of observed shear systems
7_3	0 0 1	(1 1 2)[$\bar{1}$ $\bar{1}$ 1]	0.4714	2	Slip
		(1 $\bar{1}$ 2)[$\bar{1}$ 1 1]	0.4714	8(A)	Slip
		($\bar{1}$ 1 2)[1 $\bar{1}$ 1]	0.4714	1	Slip
12_2	$\bar{3}$ 5(6 6)	(1 $\bar{1}$ 2)[$\bar{1}$ 1 1]	0.4927	8	Slip
		($\bar{1}$ $\bar{1}$ 2)[1 1 1]	0.4746	7(A)	Slip
4	$\bar{1}$ 2(2 2)	(1 $\bar{1}$ 2)[$\bar{1}$ 1 1]	0.4941	8	
		($\bar{1}$ $\bar{1}$ 2)[1 1 1]	0.4767	7(A)	Twin
		(1 1 2)[$\bar{1}$ $\bar{1}$ 1]	0.4555	2	Twin
5_3	$\bar{1}$ 3(2 0)	(1 $\bar{1}$ 2)[$\bar{1}$ 1 1]	0.4967	8(A)	Slip
		($\bar{1}$ $\bar{1}$ 2)[1 1 1]	0.4806	7	Slip
8	$\bar{1}$ 5(3 3)	(1 $\bar{1}$ 2)[$\bar{1}$ 1 1]	0.4947	8(A)	Twin
		($\bar{1}$ $\bar{1}$ 2)[1 1 1]	0.4849	7	Twin
		($\bar{1}$ 1 2)[1 $\bar{1}$ 1]	0.4109	1	Twin
11_1	$\bar{1}$ 3(1 8)	(1 $\bar{1}$ 2)[$\bar{1}$ 1 1]	0.4968	8(A)	Slip
		($\bar{1}$ $\bar{1}$ 2)[1 1 1]	0.4799	7	Slip
		(1 1 2)[$\bar{1}$ $\bar{1}$ 1]	0.4291	2(A)	Slip
6	$\bar{4}$ 9(4 9)	(1 $\bar{1}$ 2)[$\bar{1}$ 1 1]	0.4973	8(A)	Slip
		($\bar{1}$ $\bar{1}$ 2)[1 1 1]	0.4739	7	Twin
		(1 1 2)[$\bar{1}$ $\bar{1}$ 1]	0.4276	2(A)	Twin
C_2	$\bar{5}$ 6(1 6)	($\bar{1}$ 0 1)[1 1 1]	0.4598		Slip
		(0 1 1)[$\bar{1}$ $\bar{1}$ 1]	0.4250		Slip
C_{41}	$\bar{9}$(1 1)(2 0)	($\bar{1}$ 0 1)[1 1 1]	0.4327		
11_3	$\bar{8}$ 9(1 0)	($\bar{2}$ 1 1)[1 1 1]	0.3704	3	
		($\bar{1}$ 0 1)[1 1 1]	0.3299		Slip
12_1	$\bar{6}$ 6 7	($\bar{2}$ 1 1)[1 1 1]	0.3409	3	
		($\bar{1}$ 0 1)[1 1 1]	0.3070		Slip
		(0 1 1)[$\bar{1}$ $\bar{1}$ 1]	0.3070		Slip
C_1	$\bar{1}$ 1 3	($\bar{1}$ 0 1)[1 1 1]	0.4427		Slip
		(0 1 1)[$\bar{1}$ $\bar{1}$ 1]	0.4427		Slip
C_3	$\bar{3}$ 5(1 2)	(0 1 1)[$\bar{1}$ $\bar{1}$ 1]	0.4293		Slip
		($\bar{1}$ 0 1)[1 1 1]	0.4293		Slip
2_4	$\bar{1}$ 1 3	($\bar{1}$ 0 1)[1 1 1]	0.4577		Slip
		(1 $\bar{1}$ 2)[$\bar{1}$ 1 1]	0.4454	8(A)	Twin (after crack)
		(0 1 1)[$\bar{1}$ $\bar{1}$ 1]	0.4403		Slip
5_4	$\bar{1}$ 1 2	($\bar{1}$ 3 2)[$\bar{1}$ $\bar{1}$ 1]	0.4115		Slip
		(0 1 1)[$\bar{1}$ $\bar{1}$ 1]	0.4024		Slip
5_1	$\bar{5}$ 8 9	($\bar{2}$ 1 1)[1 1 1]	0.4492	3	
		($\bar{3}$ 1 2)[1 1 1]	0.4460		Slip
C_{42}	$\bar{1}$ 0(1 5)(1 8)	($\bar{2}$ 1 1)[1 1 1]	0.4427	3	
		($\bar{1}$ 0 1)[1 1 1]	0.4051		Slip
5_5	$\bar{5}$(1 0)(1 7)	($\bar{1}$ 0 1)[1 1 1]	0.4773		Slip
10_3	$\bar{1}$ 2 5	($\bar{1}$ 0 1)[1 1 1]	0.4899		Slip
3	$\bar{1}$ 3(1 0)	($\bar{1}$ 0 1)[1 1 1]	0.4899		Slip
2_3	$\bar{1}$ 3 3	($\bar{2}$ 1 1)[1 1 1]	0.4933	3	Slip
		($\bar{3}$ 2 1)[1 1 1]	0.4844		Slip
		($\bar{3}$ 1 2)[1 1 1]	0.4844		Slip
2_5	$\bar{1}$ 2 3	($\bar{3}$ 1 2)[1 1 1]	0.4834		Slip
		($\bar{1}$ 0 1)[1 1 1]	0.4535		Slip
		(1 $\bar{1}$ 2)[$\bar{1}$ 1 1]	0.2569		Twin (after crack)
5_6	$\bar{1}$ 2 5	($\bar{1}$ 0 1)[1 1 1]	0.4899		Slip
11_2	$\bar{2}$ 6 9	($\bar{1}$ 0 1)[1 1 1]	0.4825		Slip
14_2	$\bar{1}$ $\bar{3}$(2 2)(3 1)	($\bar{3}$ 1 2)[1 1 1]	0.4704		Slip
15_3	$\bar{6}$(1 1)(1 6)	($\bar{2}$ 1 1)[1 1 1]	0.4674	3	
		($\bar{1}$ 0 1)[1 1 1]	0.4567		Slip
16_3	$\bar{4}$ 7(1 0)	($\bar{2}$ 1 1)[1 1 1]	0.4643	3	
		($\bar{1}$ 0 1)[1 1 1]	0.4503		Slip
7_2	$\bar{1}$ 8 8	($\bar{2}$ 1 1)[1 1 1]	0.4933	3	
		($\bar{3}$ 1 2)[1 1 1]	0.4844		Slip
		($\bar{1}$ 0 1)[1 1 1]	0.4272		Slip
1	$\bar{1}$ 4(1 3)	($\bar{1}$ 0 1)[1 1 1]	0.4917		Slip
7_4	$\bar{1}$(1 2)(2 5)	($\bar{1}$ 0 1)[1 1 1]	0.4963		Slip
		(1 0 1)[$\bar{1}$ 1 1]	0.4835		Slip
7_1	$\bar{1}$(1 1)(1 9)	($\bar{1}$ 0 1)[1 1 1]	0.4902		Slip
		(1 0 1)[$\bar{1}$ 1 1]	0.4716		Slip
9_3	$\bar{1}$ 7(1 1)	($\bar{1}$ 0 1)[1 1 1]	0.4870		Slip
9_2	$\bar{2}$(1 0)(1 3)	($\bar{2}$ 1 1)[1 1 1]	0.4895	3	
		($\bar{1}$ 0 1)[1 1 1]	0.4711		Slip

Table I continued.

TABLE I Continued

Crystal (tensile axis)	System	Schmid factor	Schmid–Boas number	Nature of observed shear systems
9_1 $\bar{1}(10)(14)$	$(\bar{2}\,1\,1)[1\,1\,1]$	0.4746	3	
	$(\bar{1}\,0\,1)[1\,1\,1]$	0.4742		Slip
	$(1\,0\,1)[\bar{1}\,1\,1]$	0.4467		Slip
10_4 $\bar{1}\,3\,5$	$(\bar{1}\,0\,1)[1\,1\,1]$	0.4899		Slip
10_1 $\bar{2}\,7\,8$	$(\bar{2}\,1\,1)[1\,1\,1]$	0.4976	3	
	$(\bar{1}\,0\,1)[1\,1\,1]$	0.4536		Slip
10_2 $\bar{1}(45)(56)$	$(\bar{2}\,1\,1)[1\,1\,1]$	0.4703	3	
	$(\bar{1}\,0\,1)[1\,1\,1]$	0.4508		Slip
	$(1\,0\,1)[\bar{1}\,1\,1]$	0.4437		Slip
13_1 $\bar{1}\,6\,6$	$(\bar{2}\,1\,1)[1\,1\,1]$	0.4972	3	Slip
	$(\bar{3}\,2\,1)[1\,1\,1]$	0.4883		Slip
13_2 $\bar{2}(1\,1)(1\,7)$	$(\bar{1}\,0\,1)[1\,1\,1]$	0.4871		Slip
14_1 $\bar{1}\,4\,7$	$(\bar{1}\,0\,1)[1\,1\,1]$	0.4948		Slip
	$(1\,\bar{1}\,2)[\bar{1}\,1\,1]$	0.3928	8(A)	Twin (after crack)
15_2 $\bar{1}\,4\,7$	$(\bar{1}\,0\,1)[1\,1\,1]$	0.4948		Slip
	$(1\,0\,1)[\bar{1}\,1\,1]$	0.4454		Slip
16_1 $\bar{1}\,5\,7$	$(\bar{3}\,1\,2)[1\,1\,1]$	0.4979		Slip
16_2 $\bar{1}\,5\,7$	$(\bar{2}\,1\,1)[1\,1\,1]$	0.4840	3	
	$(\bar{1}\,0\,1)[1\,1\,1]$	0.4790		Slip
16_4 $\bar{1}\,8\,8$	$(\bar{2}\,1\,1)[1\,1\,1]$	0.4933	3	Slip

not be observed in crystals 11_3, 12_1 and 10_2. In order to compare the deformation behaviour of this alloy in the presence of hydrogen with that exhibited in the absence of hydrogen, two specimens, namely 15 and 16, were tested without introducing hydrogen. The slip systems observed in all the grains of specimens 15 and 16 agreed with those observed in specimens containing hydrogen for similar orientations of the tensile axis. Therefore, the presence of hydrogen did not significantly effect the deformation behaviour by slip at the two temperatures of the tensile test.

A summary of the deformation systems by slip and twinning observed in this alloy is shown in Fig. 2 for various orientations of the tensile axis. Thus, when the orientation of the tensile axis remains within any one of the regions in the standard triangle, the slip or twin systems mentioned therein are observed with a few exceptions noted previously. That plastic deformation by slip in general takes place on high index planes can be inferred from the ψ–χ curve shown in Fig. 3. A definition of ψ and χ can be found in reference [18]. For a stress axis within the 0 0 1–0 1 1–$\bar{1}$ 1 1 unit triangle, with the primary slip direction [1 1 1], χ is the angle between [$\bar{1}$ 0 1] and the normal to the plane of maximum resolved shear stress, and ψ is the angle between [$\bar{1}$ 0 1] and the observed slip plane normal. Briefly, asymmetry of slip may be deduced from the $\psi(\chi)$ curves. If there is no asymmetry, $\psi(-\chi) = -\psi(\chi)$; $\psi = 0$ for all χ which means ($\bar{1}$ 0 1) slip only; $\psi = 30°$ for $\chi > 0$ and $\psi = -30°$ for $\chi < 0$ which means {1 1 2} slip only, and $\psi = \chi$ for all χ which represents slip on maximum resolved shear stress planes. On the other hand, when asymmetry is present, it is consistent with a dependence solely on the sense of the {1 1 2} shear only if $\psi(\chi)$ in tension equals $-\psi(-\chi)$ in compression. It can be concluded from the above brief comments found in [18] that slip in this alloy is asymmetric and depends on the sense of {1 1 2} shear. The latter conclusion can be reached by comparing the results of Fig. 3 with the results presented in [18] (Fig. 10) wherein the $\psi(\chi)$ curve is drawn for a niobium–5 at % molybdenum alloy tested under compression at 295 K. The recent experimental work by the author (results to be published) has shown that

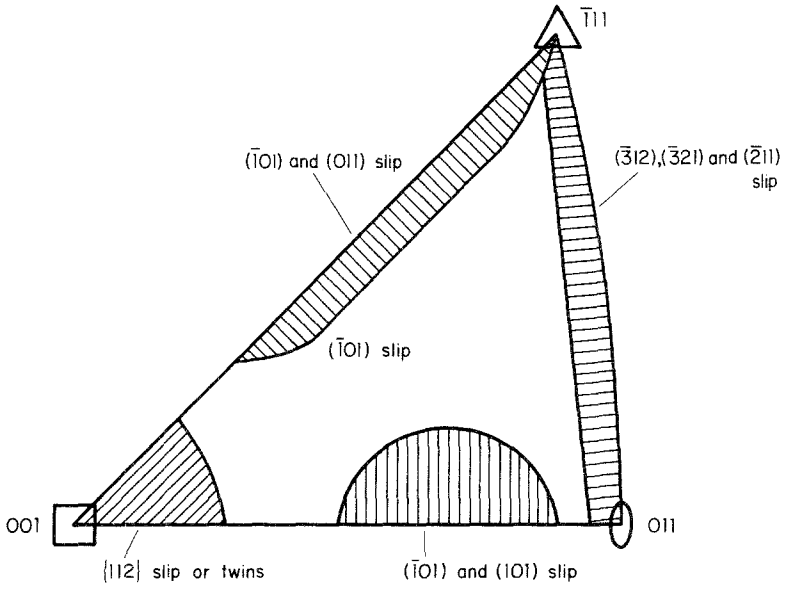

Figure 2 A schematic illustration of the slip or twin systems observed in the niobium-rich niobium–vanadium alloy containing hydrogen in solid solution.

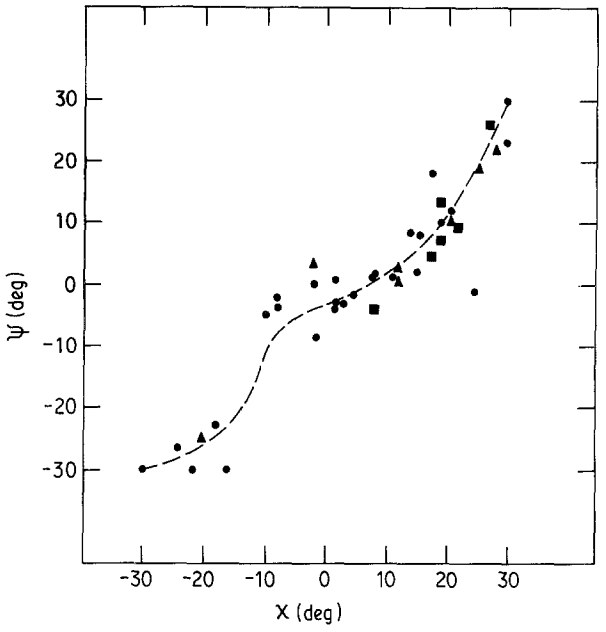

Figure 3 $\psi(\chi)$ curve drawn from the observed slip systems in the niobium–10 at % vanadium alloy deformed in tension. See [18] for the definition of ψ and χ. (●) 195 K hydrogen, (▲) 295 K hydrogen, (■) 195 K no hydrogen.

the plastic deformation behaviour by slip of a niobium–10 at % vanadium alloy is similar to that exhibited by a niobium–10 at % molybdenum alloy. It is also clear from the results shown in Fig. 3 that the presence of hydrogen has not significantly changed the $\psi(\chi)$ curves. Thus the data points corresponding to the specimens without hydrogen are found to remain close to the results applicable to other specimens with hydrogen.

It is now useful to consider the origin of deformation twins observed in this alloy. Ideally, at sufficiently low temperatures and as a function of alloying, twinning as the deformation behaviour is favourable for the orientation of the tensile axis close to the 0 0 1 pole. However, it can be inferred from Fig. 2 and from the results presented in Table I, that the observed deformation behaviour is not entirely by twinning except in Specimen 4 where twinning is associated with a (0 0 1) cleavage crack. The engineering stress against strain curve for Specimen 4 is shown in Fig. 1. Deformation twinning observed in all crystals of this alloy is associated with cracks formed in specimens tested only at 195 K. First, it is important to clarify if hydrogen is responsible for the observed deformation twins. Second, it is necessary to know if the twins are responsible for the nucleation of cracks or vice versa.

A reference to vacuum fusion analysis of the samples for hydrogen, oxygen and nitrogen mentioned earlier does not lead to the conclusion that either higher or lower amounts of hydrogen were responsible for twinning. Thus, for example, Crystals 4 and 6 did not contain as much hydrogen as Crystals 11_1 and 12_2 but still exhibited twinning. Similarly, if it were the smaller quantities of oxygen [6], this is certainly not true in Specimen 8 where the largest amount of oxygen in this series was found but deformation twinning is observed. The twins observed in other specimens tested at 195 K such as 14_1, 2_5 and 2_4 are also associated with the presence of cracks. The fractographic observations of the fracture behaviour of this alloy will now be presented to determine the relationship between twins and nucleation of cracks and also the general fracture behaviour of this alloy.

The traces of twins on the two parallel surfaces of Specimen 4 shown in Figs 4a and b illustrates that the set of twins observed on one side of the crack is not present on the other side (see Fig. 4a), whereas a different set of twins is seen indicating that the crack has formed before the twins. This observation is also partially in concurrence for the two twin traces observed in Fig. 4b. It is possible that the two sets of twins are the non-crossing type and that one set of twins has formed before the other. However, twins seen in Crystals 4, 6 and 8 with tensile axis close to the 0 0 1 pole are observed only in the presence of a (0 0 1) crack. A few other crystals, 7_3, 11_1 and 12_2 with orientation of the tensile axis close to the 0 0 1 pole have not deformed by twinning. In order to further prove that twins are not responsible for the nucleation of cracks, a numerical analysis based on discrete dislocation modelling of cracks and twins is presented in the discussion of the results. Furthermore, twinning as the deformation behaviour may be expected only at much lower temperatures, close to 77 K and below in this alloy.

Fig. 5 illustrates the plastic deformation due to stress concentration associated with the terminating twins which propagated from the crack surface [33–35]. Similarly, Fig. 6 illustrates twins which are situated opposite to each other before terminating and coalescing to form plastically deformed regions parallel to twin orientation in between [36]. These metallographic features illustrate that twinning in this material is similar to deformation twinning in other systems including other niobium–vanadium alloys. Similar observations of twins associated with a (0 0 1) cleavage crack are also made in Specimens 6 and 8. The scanning electron microscopic observations of one of the fracture surfaces of Specimen 4 shown in Fig. 6 illustrate the formation of both the twin traces on the fracture surface except at one corner where twin traces are absent. This evidence suggests that the cleavage crack has nucleated in this region and propagated with the formation of twins on either side in the manner originally proposed by Orowan [37]. Using electron channeling, it has been shown qualitatively by the author that plastic deformation is confined to a few micrometers on either side of the crack surface.

In addition to the (0 0 1) type cleavage, cracks along {1 1 2} and {1 1 0} type planes are also observed in this alloy crystals in the presence of hydrogen. Thus, crystal 7_3 which deformed by slip failed by cracks along the $(\bar{1}\,1\,2)$ slip planes, as shown in Fig. 7. The crack planes are stressed in combined tension and shear and not in pure tension. Apparently, these mixed mode cracks are formed along the slip planes as a result of a large accumulation of hydrogen atoms at the stress concentration of deformed regions associated with slip bands causing easy separation of atomic planes. The displacements perpendicular to the

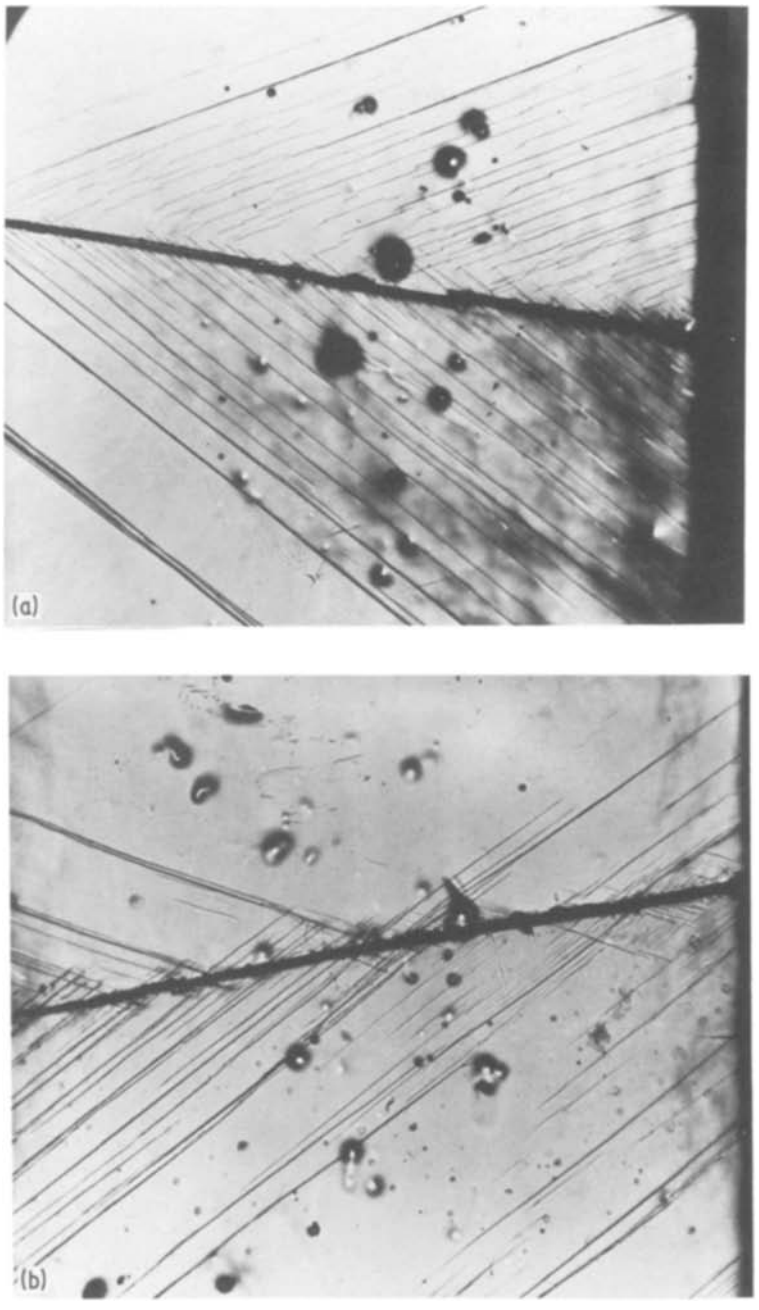

Figure 4 (a) Optical micrograph showing the traces of a crack parallel to a (0 0 1) plane and two intersecting twins parallel to (1 1 2) planes on the surface in a single crystal of Specimen 4. The Schmid–Boas numbers of the twins are 2 and 7. (Magnification: 48 ×). (b) Optical micrograph showing the traces of a crack parallel to a (0 0 1) plane and two intersecting twins parallel to (1 1 2) planes on the second surface opposite to that in Fig. 4a. (Magnification: 48 ×).

crack faces provide the free surface for adsorption of hydrogen atoms [38, 39] which in turn leads to easier propagation of microcracks. Of these, a few cracks are seen in Fig. 7 to be stopped by the grain boundary but two of the cracks propagated across. The cracks continued to be in shear in the adjacent grains where the cracks propagated along the (1 1 0) type slip planes. Similar behaviour is observed in Crystal 12_2, where a tensile crack initially propagated along the (0 0 1) plane but changed into a mixed mode crack close to the (1 $\bar{1}$ 2) plane without the necessity to nucleate twins to relieve stress concentration.

An example of cracks parallel to the ($\bar{1}$ 0 1) slip planes is shown in Fig. 8. These mixed mode cracks parallel to the ($\bar{1}$ 0 1) slip plane are formed as a result of coalescence of several microcracks that are inclined to the major crack, as shown in Fig. 9. The plastic deformation associated with the cracks nucleated along either the {1 1 2} or {1 0 1} type slip planes is sufficiently large to prevent catastrophic brittle fracture. There is enough experimental evidence [40] to suggest that dislocation cell walls formed in the deformed regions of the slip bands become the nucleation centres for cracks.

Figs 10a and b illustrate the grain boundary triple point on two opposite and parallel faces wherein fracture initiated in Specimen 2. In these figures, Crystal 2_4 is on the left hand side while Crystal 2_5 is on the top right hand side in Fig. 10a and on the bottom right side in Fig. 10b. The Crystal 2_4 failed by a mixed mode (0 0 1) crack. On the other hand, the crack in Crystal 2_5 propagated along ($\bar{1}$ 1 2) in Fig. 10b while it propagated along the ($\bar{1}$ 0 1) slip plane in Fig. 10a. Thus, there was a step formed on the crack surface between the opposite faces of the specimen. The ($\bar{1}$ 1 2) type crack is more tensile oriented than the mixed mode ($\bar{1}$ 0 1) crack which nucleated at the grain-boundary triple point. In Specimen 14, both an intergranular crack (Fig. 11) and a transgranular crack (Fig. 12) are observed. However, only the (0 0 1) mixed

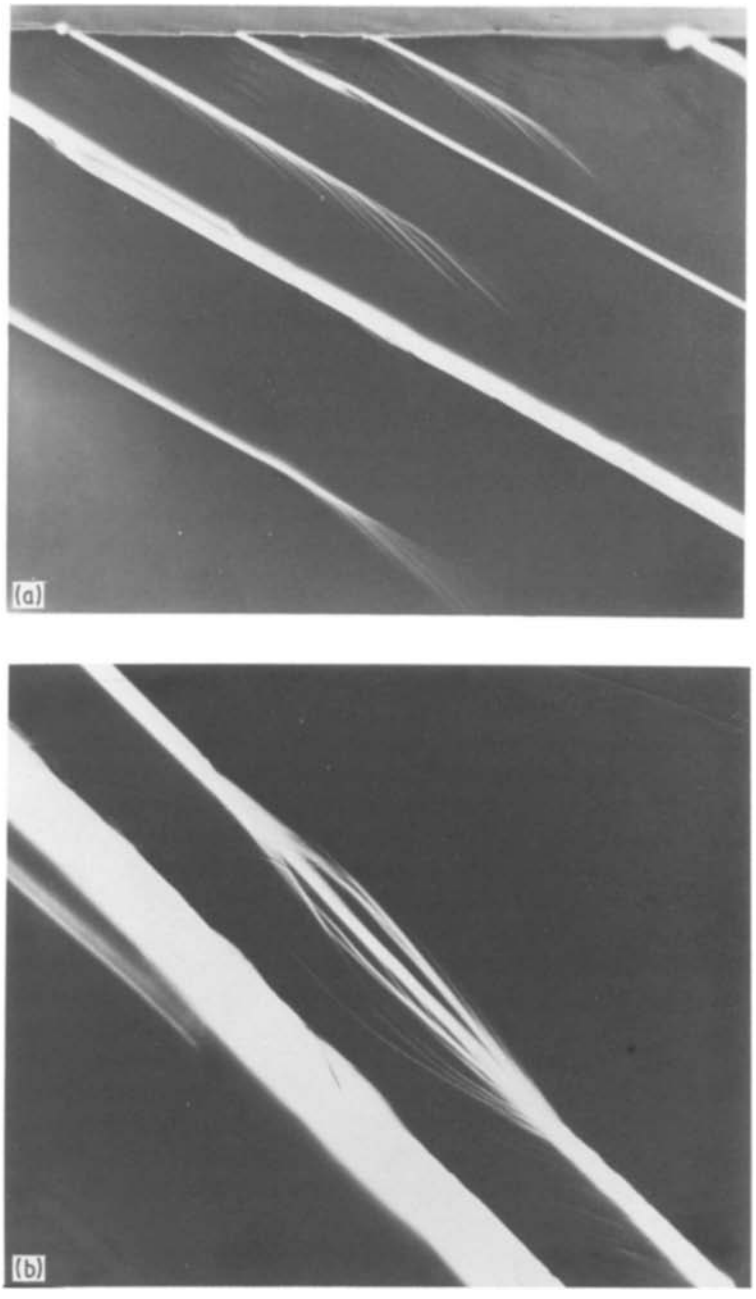

Figure 5 (a) Optical micrograph showing the plastic deformation associated with (1 1 2) type twins terminating in Crystal 4. The twins are intersecting a (0 0 1) crack surface. (Magnification: 1280 ×). (b) Optical micrograph showing the plastic deformation associated with two (1 1 2) type twins terminating in Crystal 4 opposite to each other. (Magnification: 2000 ×).

mode transgranular crack propagated suggesting that the grain boundaries are relatively stronger in this alloy, a result which will be useful to explain the large ductility exhibited by this alloy. The formation of an intergranular crack shown in Fig. 11 is the only observation of such type in several crystals of this alloy deformed in tension. Both Specimens 2 and 14 showed fracture across a grain-boundary triple point where a crack could be nucleated due to the absence of sufficient number of slip systems needed to maintain the continuity of the material.

A summary of the observed crack planes in this alloy in the presence of hydrogen is shown in Table II. In addition to cracks observed along the (0 0 1) cleavage, the {1 1 2} and the {1 0 1} type slip planes, there are cracks observed along {1 1 2} and {1 0 1} type planes on which no slip is observed. However, the normal component of stress responsible for cracks on these planes, estimated from the orientation of the tensile axis, is found to be fairly high. Apparently, while the nucleation mechanism [41–43] of the (0 0 1) cleavage cracks by the combination of dislocations in the form

$$a[1\,1\,\bar{1}]/2 + a[1\,\bar{1}\,1]/2 = a[1\,0\,0] \qquad (1)$$

where a is the lattice parameter, can be invoked, such a mechanism while possible in Crystals C_1 and C_3 has not been responsible for any (0 0 1) cracks. Presumably, this result arises due to the smaller component of applied stress that is unable to open the crack faces by coalescence of the dislocations with Burgers vector of $a[0\,0\,1]$ type which are prevented from further movement in the lattice.

It is important at this point to mention the effect of an additional electrolytic polishing step after charging with hydrogen. Therefore higher concentrations of hydrogen adsorbed locally at the free surface are removed. Specimens 2, 3, 13 and 14 which were mechanically and electrolytically polished after charging with hydrogen showed extensive deformation except Specimen 13 in which an intergranular crack developed near the pin hole. Specimens 4, 6 and 8 could be

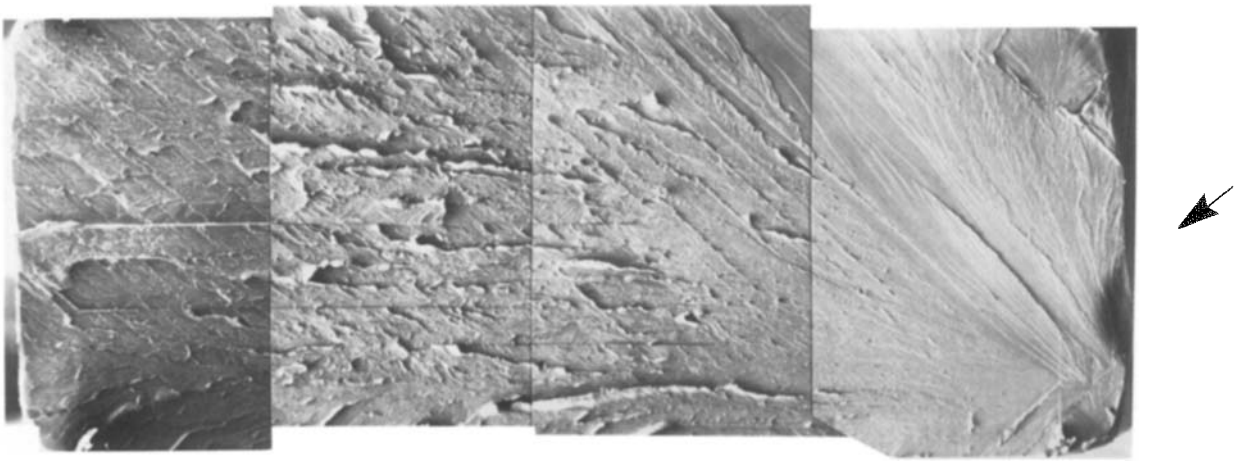

Figure 6 Scanning electron microscopic observations of the fracture surface of the (0 0 1) crack showing the two twin traces and the transgranular cleavage in Specimen 4. The arrow points to the region where nucleation of the crack has been identified. (Magnification: 56 ×).

set aside because of their specific orientation favourable for a (0 0 1) cleavage and thus can not exhibit any plastic deformation. On the other hand, it has been found that the total strain before fracture in Specimens 2, 3 and 14 is larger by about 10 to 15% compared to the total strain in other specimens. This difference in elongation is attributed to the removal of the surface layers containing higher hydrogen concentration. The author believes that early formation of cell structure in the presence of a high concentration of hydrogen near the surface is responsible for the nucleation of cracks.

Several polycrystalline small grain size samples designed for pin loading were prepared following the same procedure mentioned earlier and were charged with 200, 400 and 600 p.p.m. wt hydrogen. Metallographic examination of the specimens tested in tension at three temperatures, namely 77, 195 and 295 K revealed the presence of no deformation twinning prior to fracture. The embrittled fracture surface of a specimen charged with a nominal 600 p.p.m. wt hydrogen and tested in tension at 195 K is examined in the secondary electron emission method in the scanning electron microscope. The result shown in Fig. 13 illustrates again the absence of intergranular fracture. However, the twins observed in the same specimen remain very close to the path of the crack, as seen in the optical micrograph shown in Fig. 14.

4. Discussion

The results of experiments on single crystals and polycrystals of large grain size of the niobium-rich vanadium alloy indicate that provided the {1 1 2}, {1 0 1} and {3 2 1} planes are considered as the possible slip planes, Schmid's law is very much followed, namely slip or twinning on maximum resolved shear stress planes is observed with the exception that $(\bar{2}\,1\,1)$ [1 1 1] slip system is present only when the orientation of the tensile axis is either on the $\bar{1}\,1\,1$–0 1 1 border or very close to it. Similarly, slip on $(\bar{3}\,2\,1)$ or $(\bar{3}\,2\,1)$ planes appears only at room temperature for crystals with orientation close to $\bar{1}\,1\,1$ pole. Further, both the $(\bar{1}\,0\,1)$ and (1 0 1) slip planes are observed in the presence of hydrogen only when the orientation is close to the 0 0 1–0 1 1 border. On the other hand, both these slip systems are observed for orientations away from the border also in the absence of hydrogen. Thus, there is no significant effect of hydrogen on the crystallographic deformation behaviour of this alloy.

Plastic deformation by slip in this alloy in general

TABLE II Crystals where cleavage on (0 0 1) plane by combination of a[1 1 1]/2 dislocations or where crack formation on (1 1 0) or (1 1 2) type plane along deformation bands is possible shown with the actually observed crack plane

Crystal	Is (0 0 1) cleavage possible?	Is there a deformation band on the crack plane?	Observed plane of the crack	Mode of applied stress
4	yes	no	(0 0 1)	Tension
6	yes	no	(0 0 1)	Tension
8	yes	no	(0 0 1)	Tension
12_2	no	yes	$(1\,\bar{1}\,2)$	Tension and shear
12_2	yes	no	(0 0 1)	Tension
7_3	yes	yes	$(\bar{1}\,1\,2)$	Tension and shear
C_1	yes	no	$(\bar{1}\,1\,2)$	Tension
C_3	yes	yes	(0 1 1)	Tension and shear
C_{42}	no	no	$(\bar{1}\,1\,2)$	Tension
2_4	yes	no	(0 0 1)	Tension and shear
2_5	no	yes	$(\bar{1}\,0\,1)$	Tension and shear
2_5	no	no	$(\bar{1}\,1\,2)$	Tension and shear
11_2	no	no	(0 1 1)	Tension and shear
14_1	no	no	(0 0 1)	Tension and shear
1	no	yes	$(\bar{1}\,0\,1)$	Tension and shear

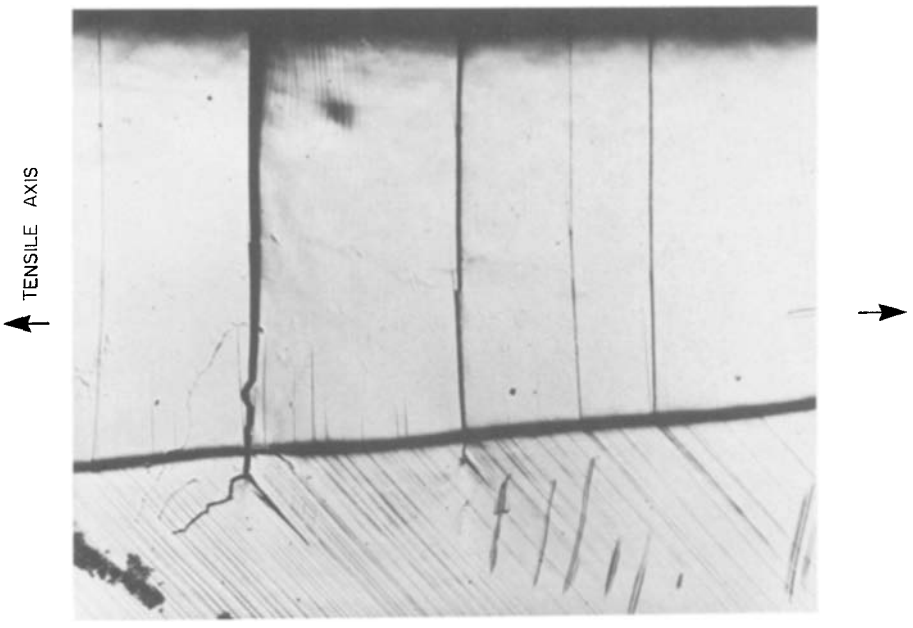

Figure 7 Optical micrograph showing cracks parallel to a (1 1 2) type plane in the upper grain 7_3 and parallel to a (1 1 0) type plane in the lower grain 7_1 in Specimen 7. (Magnification: 24 ×).

appears to be on high index planes in concurrence with the observations on other bcc metals and alloys [19]. Thus $\psi(\chi)$ curves are considered as a better representation of the deformation behaviour of this alloy. The results shown in the form of a $\psi(\chi)$ curve illustrated the presence of asymmetry as well as the dependence on the sense of $\{1\,1\,2\}$ shear.

The fracture behaviour of this alloy with hydrogen is complex in the sense that in addition to the (0 0 1) cleavage observed in all bcc metals and alloys, both the (1 1 2) and (1 1 0) type crack planes are also observed. It is clear from the results presented in Table II that crack formation in the presence of hydrogen can be reasoned in terms of three or four simple mechanisms. Thus, when dislocations of suitable Burgers vector combine to form dislocations with Burgers vector $a[0\,0\,1]$, and the component of normal stress on the (0 0 1) crack planes is high, the familiar Stroh or Cottrell mechanism [41, 42] explains the formation of cracks. On the other hand, when a combination of normal and shear stress components is acting on the slip planes, accumulation of hydrogen along cell walls formed parallel to the severely deformed regions explains the crack formation. Crack nucleation at triple point grain-boundary junctions due to the absence of sufficient number of slip systems is yet another mechanism that explains certain results shown in Table II namely in Specimens 2_5 and 14_1. Finally, the mechanism involving microslip or formation of cell structure along close packed planes which are not the operating slip planes and thus giving rise to a stress concentration that can lead locally to a higher hydrogen concentration and attendant crack nucleation appears to explain the other types of cracks illustrated in Table II, namely in specimens C_1 and C_{42}. In particular, it is found that a higher value of the normal component of applied stress helps this mechanism of crack nucleation.

At this point, it is useful to analyse the nucleation of twins and cracks in this alloy in the presence of hydrogen. In particular, the energy associated with the nucleation of a twin lamalla is calculated to determine

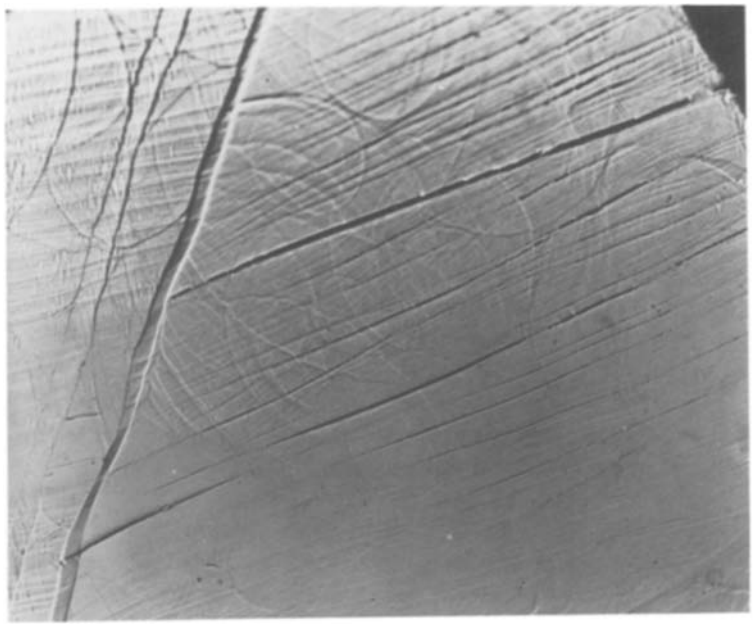

Figure 8 Transgranular cleavage cracks parallel to the $(\bar{1}\,0\,1)$ slip planes terminating at a grain boundary in Specimen 1. (Magnification: 150 ×).

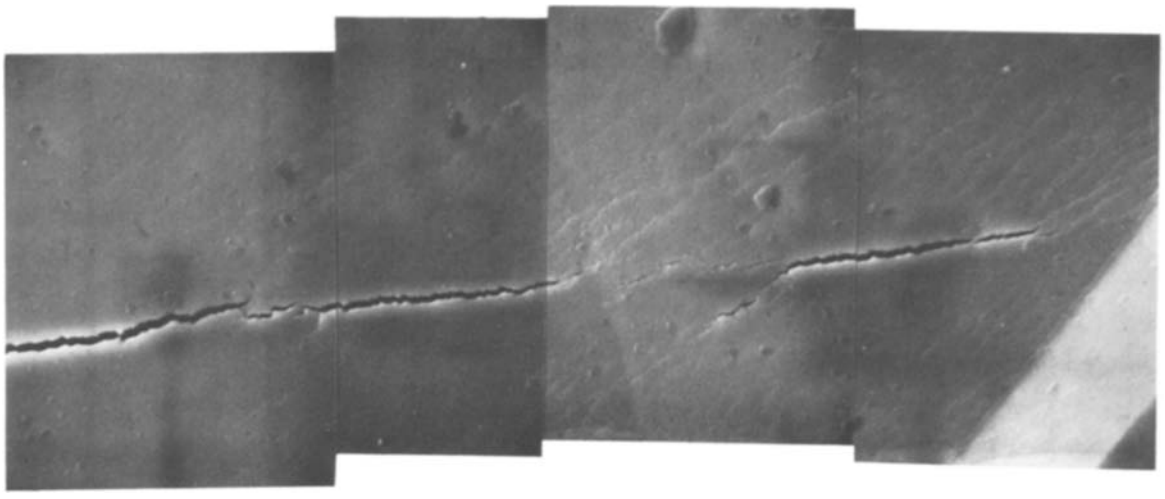

Figure 9 Scanning electron micrograph showing the coalescence of several microcracks to form a major crack parallel to the slip plane in Specimen 1. (Magnification: 200 ×).

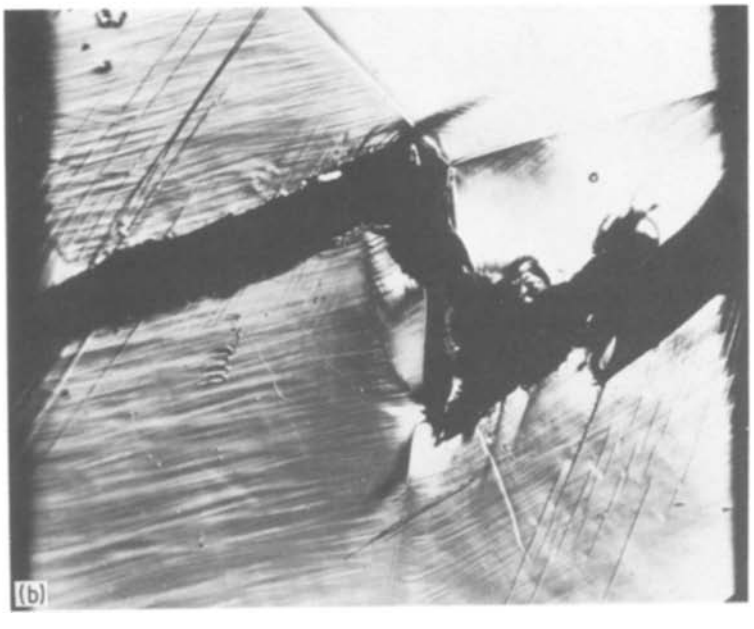

Figure 10 (a) Optical micrograph showing a crack nucleated along a grain boundary at the triple point but propagated transgranularly in Specimen 2. Crystal 2_4 is on the left hand side while Crystal 2_5 is on the top right and Crystal 2_3 is on the bottom right. (Magnification: 96 ×). (b) Optical micrograph showing a crack nucleated along a grain boundary at the triple point but propagated transgranularly in Specimen 2. Same as Fig. 10a but the opposite parallel surface is shown. Crystal 2_4 is on the left hand side while Crystal 2_5 is on the bottom right and Crystal 2_3 is on the top right. (Magnification: 96 ×).

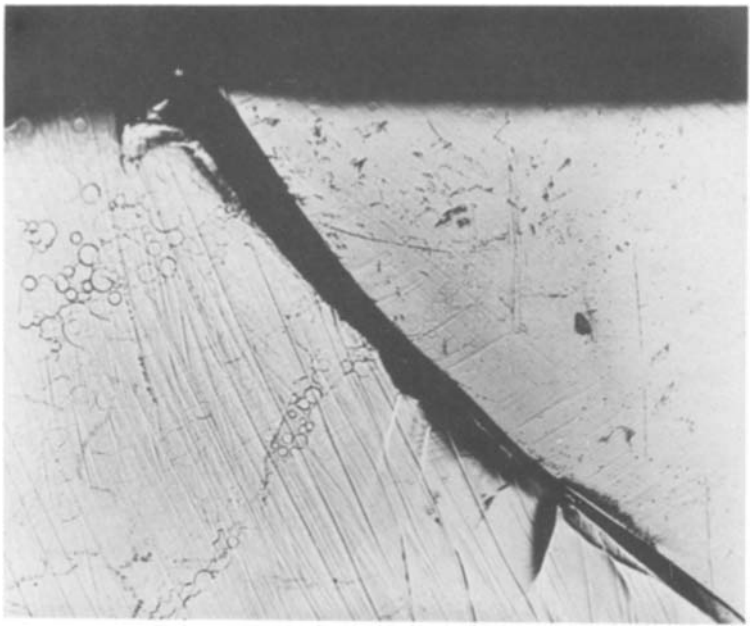

Figure 11 A crack along a grain boundary which did not propagate to fracture in Specimen 14. (Magnification: 120 ×).

the critical size of the twin that can grow with decreasing energy under the action of the applied stress. The purpose of the present calculations is to show that the activation energy for the nucleation of twins is sufficiently high that only a stress concentration due to a crack or an array of straight lattice dislocations under high lattice frictional stress can be responsible for twinning. The twin lamella is modelled as shown in Fig. 15 where the twinning dislocation loops with Burgers vector $\boldsymbol{b}_t = a[1\,1\,1]/6$ move on the $(\bar{1}\,\bar{1}\,2)$ type twinning planes with the interplanar distance given by $a[\bar{1}\,\bar{1}\,2]/6$ and $a = 0.330\,07$ nm. The component of applied stress acting on the twinning dislocations becomes $\tau = 0.4714\sigma_a$ where σ_a is the tensile stress acting in the [0 0 1] direction and the Schmid's factor, $m = 0.4714$ shown in Table I is used. In particular, the total energy of the configuration of the twin lamella is given by

$$E_T = E_e + E_{\gamma_T} \tag{2}$$

In the above E_e is the elastic energy released in the formation of the twin, E_{γ_T} the twin boundary energy given by $2\pi R_0^2\gamma_T$, where R_0 is the size of the twin lamella and γ_T the twin boundary energy per unit area. On the other hand, the elastic energy associated with the twin is

$$E_e = E_S + E_I - E_W + E_F \tag{3}$$

where E_S is the self energy, E_I the interaction energy, E_F the work done against the frictional stress and E_W the work done by the applied stress, all associated with the twinning dislocations. The expressions for E_S and E_I are readily available [44]. On the other hand, E_W is given by

$$E_W = 2\pi \sum_{i=1}^{n} (R_i^2 - \boldsymbol{b}_t^2)\tau\boldsymbol{b}_t \tag{4}$$

while E_F is obtained by replacing τ by τ_f in Equation 4. In order to determine the equilibrium configuration of the twin, the energy E_e is minimized with respect to the positions of the twin dislocations. The number of twinning dislocations is incremented in the minimiza-

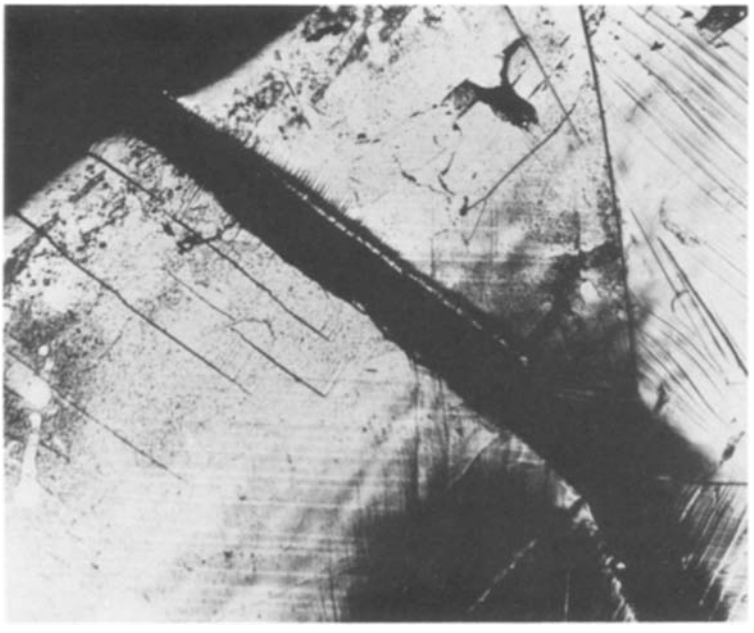

Figure 12 A transgranular cleavage crack nucleated at the grain boundary triple point but propagated along the (0 0 1) plane in Crystal 14_1 in Specimen 14. (Magnification 37.5 ×).

Figure 13 Scannning electron micrograph showing the transgranular cleavage fracture surface of a small grain size polycrystalline specimen with a nominal 600 p.p.m. wt hydrogen tested at 77 K.

tion as long as the total energy, E_e decreases for a given size of the twin. The details of the minimization program are provided in detail elsewhere [45]. After the energy of the twin for an initial size is determined, in the next step, the size is incremented and the energy determined again. Finally, when the total energy reaches a maximum and decreases with further increment of twin size, R_0 the Griffith configuration of the twin is obtained. The Griffith configuration of size, R_T corresponds to the metastable situation above which the twin propagates continuously with decreasing energy and below which it contracts to zero size. All numerical calculations presented in this paper were carried out on the Digital Vax 780 system using the elastic constants which correspond to the niobium–10 at % vanadium alloy. In order to arrive at the elastic constants of this alloy and in the absence of available data, a linear variation between that of the pure components is assumed. Thus, the shear modulus, $G = 4.037 \times 10^4$ MPa and the Poisson's ratio, $\nu = 0.388$ have been used while the twin boundary energy, $\gamma_T = 100\,\text{ergs}\,\text{cm}^{-2}$ is employed in the numerical calculations. An experimental estimation of the twin boundary energy, γ_T is hitherto not available for this alloy. The applied stress which corresponds to that observed in Specimen 4 namely $\sigma_a = 346.5$ MPa has been used which gives $\tau = m\sigma_a = 163.3$ MPa while τ_f has been varied [45] from zero to 86.6 MPa. Thus the presence of increasing amounts of hydrogen which raises the yield stress in the material [20], also increases frictional stress, τ_f to movement of dislocations preventing slip and thereby presumably induces twinning to be the deformation behaviour. The influence of hydrogen on deformation twinning can be determined with the above parameters used in the numerical calculations and the size of the Griffith configuration R_T determined.

The results of numerical calculations are shown in Table III where the energy terms contributing to the total energy, E_T are listed as a function of τ_f. In the consideration of the equilibrium of the configuration of the twin, it is possible to develop the constitutive energy equations [45] which relate the various energy terms in Table III; namely

$$E_S + E_I = (E_W - E_F)/2 \quad (5)$$

so that

$$E_e = -(E_W - E_F)/2 \quad (6)$$

a result which is verified within the accuracy of the discrete dislocation analysis. The size of the Griffith configuration of the twin above which the twin propagates with decreasing total energy, E_T is shown in Fig. 16 as a function of the frictional stress, τ_f. Also shown in Fig. 16 as a function of γ_S is the size of the Griffith configuration of an elastic circular crack, R_C which can propagate in a brittle manner; given by [46]

$$R_C = \pi G\gamma_S/\sigma_a^2(1 - \nu) \quad (7)$$

where γ_S is the free surface energy. The adsorption of hydrogen atoms on the crack surfaces reduces the surface energy [38, 39] thus reducing the size of the Griffith crack, R_C. The critical size of the twin, R_T is seen to increase with increasing τ_f illustrating that both slip and deformation twinning are suppressed in the same manner. On the other hand, the critical size of the Griffith crack, R_C decreases whereas that of the twin, R_T increases with increasing concentration of hydrogen in solid solution. In the absence of slip, deformation twinning becomes inevitable if work done by the applied stress reaches a value at which the activation energy is reduced to a negligible value. The results of Fig. 16 also illustrate that twinning can not be observed in the polycrystalline fine grain size alloy

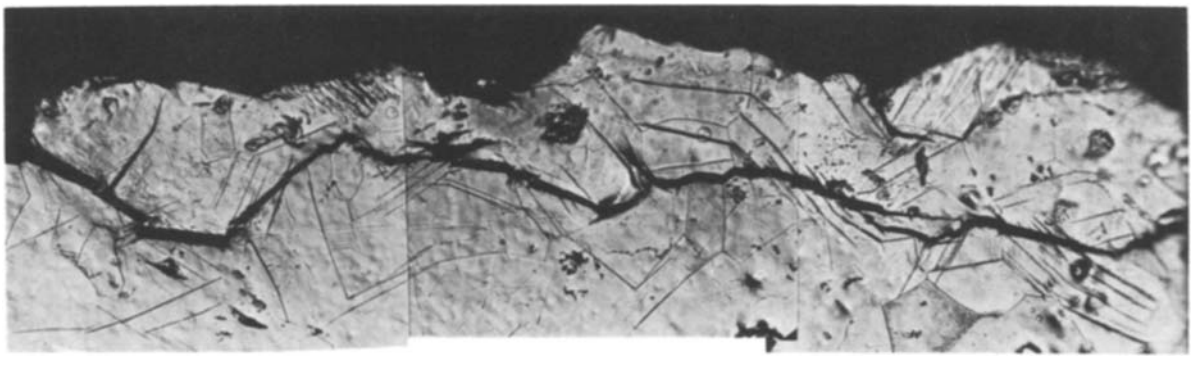

Figure 14 Optical micrograph showing the transgranular path followed by a secondary crack parallel to the fractured surface in a small grain size polycrystalline specimen with a nominal 600 p.p.m. wt hydrogen tested at 77 K.

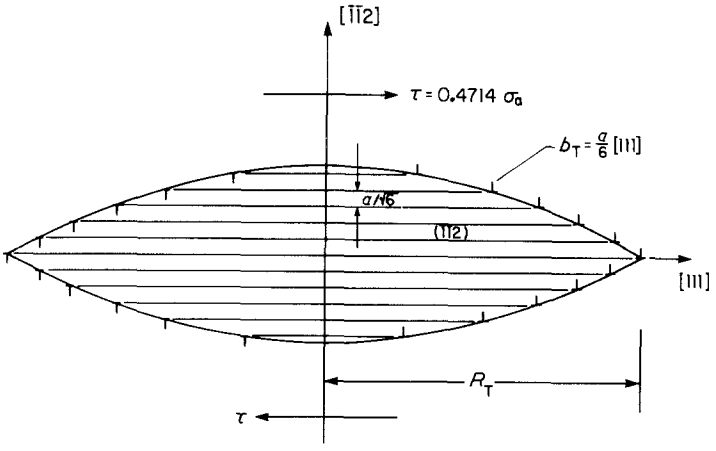

Figure 15 A schematic illustration of the dislocation model used to represent a twin lamalla at the Griffith configuration of size, R_T. The two dislocations of opposite sign on the twinning planes represent circular dislocation loops with Burgers vector $\boldsymbol{b}_t$.

in the presence of hydrogen unless the grain size is larger than the critical size of the twin, a result experimentally verified [6–8, 10], in particular since R_T is already shown to be a function of τ_f or the hydrogen concentration.

The activation energy required to nucleate a stable twin, R_T shown in Fig. 17 increases as a function of τ_f making twinning a difficult process of deformation. However, the activation energy is strongly dependent on the stress field of interaction and thus for this reason, stress concentration due to microslip has been invoked earlier in the literature [47]. Thus, in the presence of stress concentration due to straight dislocations formed during microslip, the activation energy required for twinning is reduced so that deformation twinning becomes possible. At the same time, experimental observations illustrate that prior straining at a higher temperature reduces the tendency for twinning during subsequent deformation at a lower temperature [48]. Therefore, only microslip which indicates strains much smaller than can suppress twinning is considered responsible for stress concentration that reduces the activation energy [47]. It is believed that introduction of a more uniform dislocation substructure suppresses twinning [49] but straight dislocation arrays formed during the regime of microslip provide enough stress concentration so that the activation energy required for twinning is reduced.

An additional parameter on which the critical size, R_T and the activation energy, E_T are strongly dependent is the twin boundary energy, γ_T which usually decreases with the addition of alloying elements. In order to determine the effect of hydrogen on the stacking fault energy and thus the twin boundary energy, the dislocation substructures developed in this alloy are examined at different wt % of hydrogen. Whereas the results are to be presented subsequently, there is no evidence to suggest that hydrogen in solution reduces, γ_T to a value at which twinning becomes possible. On the other hand, the presence of straight dislocations parallel to each other indicates a high value of τ_f, and also the development of stress concentration necessary for twinning. Thus far, the above experimental results and computer modelling lead to the conclusion that twinning observed in this alloy at 195 K is a result of a high stress concentration developed at the tip of a cleavage crack formed in the presence of hydrogen. A fast propagating cleavage crack requires a high strain rate deformation at the tip which can be accommodated by deformation twinning. On the other hand, the stress concentration due to arrays of straight dislocations in the regime of microslip is responsible for twinning at much lower temperatures, namely 77 K.

It is now useful to turn our attention to transgranular against intergranular crack formation in this alloy in the presence of hydrogen in solid solution. Two experimentally established results will be used in understanding this phenomenon. Firstly, adding vanadium to niobium rapidly increases the solubility of hydrogen supposedly by the trapping of hydrogen

TABLE III Energy contributions associated with the total energy of a nucleated twin lamella at the Griffith configuration as a function of frictional stress, τ_f. The applied stress, σ_a = 346.5 MPa, the orientation factor, m = 0.4714 and the twin boundary energy, γ_T = 100 erg cm^{-2}. The energy terms are in given units of 10^{-6} ergs

	τ_f (MPa)				
	0	21.65	43.30	64.95	86.60
R_T (A)	3,000	3,400	6,000	8,400	12,600
E_S	0.0788	0.0989	0.2333	0.4229	0.8094
E_I	0.3082	0.4136	1.1910	2.6420	6.0990
$E_S + E_I$	0.3870	0.5125	1.4243	3.0649	6.9084
E_W	0.7892	1.0940	4.2710	10.3700	28.4900
E_F	0	0.1161	1.3590	4.4020	15.1100
$(E_W - E_F)/2$	0.3946	0.4890	1.4560	2.9840	6.6900
E_e	−0.4022	−0.4599	−1.4880	−2.9110	−6.4800
E_{r_T}	0.5657	0.7266	2.2630	4.4350	9.9792
E_T	0.1635	0.2607	0.7750	1.5240	3.4992

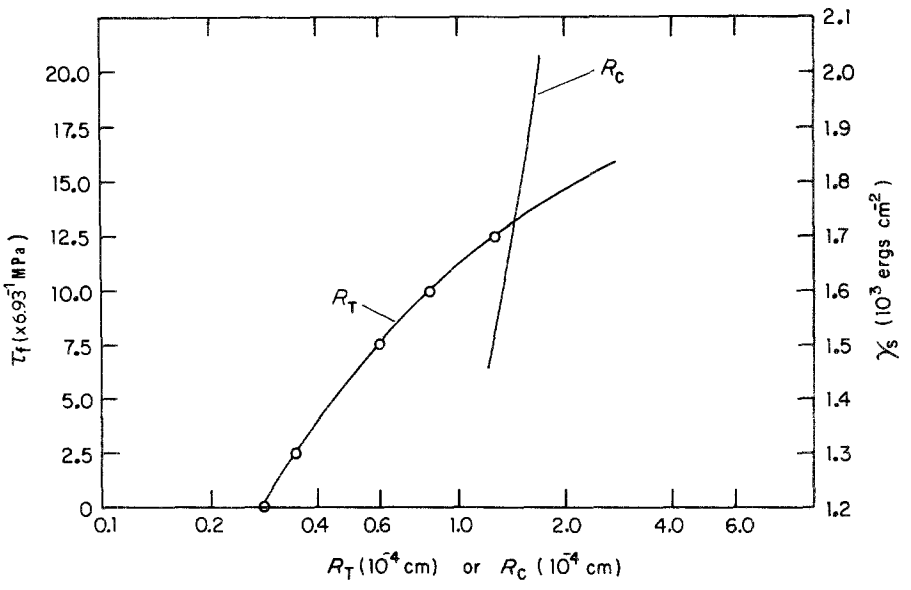

Figure 16 The Griffith size of a twin lamalla, R_T shown as a function of the frictional stress, τ_f. Also, shown is the size of a Griffith circular crack as a function of the free surface energy γ_S. σ_a = 346.5 MPa, m = 0.4714, γ_T = 100 ergs cm^{-2}.

to vanadium atoms [50] and in addition the grain-boundary surface energy decreases with increasing adsorption of hydrogen on the grain boundary surfaces [38]. Secondly, intergranular cracks are easily nucleated in higher vanadium alloys and very rarely observed in niobium-rich alloys. A close analogy with grain-boundary embrittlement in ordered alloys is thought useful [51, 52]. Let us for instance imagine the atomic 50Nb–50V alloy as consisting of perfectly arranged niobium and vanadium atoms represented by A and B atoms respectively at the grain boundary similar to that in an ordered alloy (see the grain boundary structure illustrated in [51]). It is clear that with the trapping of hydrogen to vanadium atoms, the nature of the bonds is disturbed severely at a few positions along the grain boundary. In addition, the adsorption of hydrogen at the grain-boundary surfaces is more effective as a result of trapping of hydrogen to vanadium atoms. While in a disordered alloy, the regular arrangement of atoms similar to that in an ordered alloy is absent, the weakening of the grain boundary for the above mentioned reasons is very effective. Thus, intergranular crack nucleation is very much easier in higher vanadium alloys due to the larger number of vanadium atoms at the grain boundary [10]. Very few grain-boundary cracks have been observed in niobium-rich alloys for the same reason. This result also explains the higher ductility of the present niobium-rich alloy.

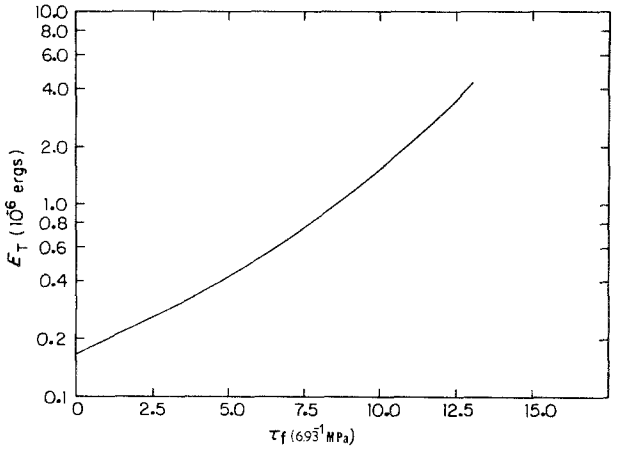

Figure 17 The activation energy, E_T associated with a twin lamalla shown as a function of the frictional stress, τ_f. σ_a = 346.5 MPa, m = 0.4714, γ_T = 100 ergs cm^{-2}.

5. Conclusions

The deformation and fracture behaviour of hydrogen embrittled niobium-rich vanadium alloy studied in tension using single crystals and large grain size polycrystals at 195 and 295 K resulted in the following conclusions.

1. Schmid's law, i.e. slip or twinning on planes with maximum resolved shear stress has been found to be followed in the nature of deformation of this alloy crystals in the presence of hydrogen with a few exceptions. The presence of hydrogen in solid solution has no significant effect on the deformation behaviour of single crystals.

2. Twinning observed with hydrogen in solid solution of this alloy at 195 K is a result of stress concentration around the crack tip.

3. Crack nucleation in this alloy has been identified under the following four mechanisms; (a) the familiar Stroh or Cottrell mechanism of (0 0 1) cleavage, (b) the nucleation of cracks along deformation bands or cell walls formed along the slip planes, (c) the nucleation of cracks in the regions of stress concentration due to microslip and (d) the nucleation of cracks at the grain-boundary triple points due to absence of sufficient number of slip systems. The cracks remained mostly close to the {0 0 1} or {1 1 2} or {1 1 0} type planes. On the other hand, the plastic deformation associated with cracks on the {0 0 1} planes is much smaller than that associated with cracks on {1 1 0} or {1 1 2} planes.

4. The trapping of hydrogen by vanadium to increase adsorption and the development of severely distorted bonds across grain boundary surfaces is used to explain the tendency for nucleation of intergranular cracks in the higher vanadium alloys. On the other hand, the higher ductility of niobium-rich alloys is considered to be the result of the absence of the above mechanisms of grain-boundary weakening.

Acknowledgements

The author wishes to take this opportunity to thank the scientific staff of the Ames Laboratory for useful discussions. In particular, the help of Mr Charles V. Owen and Edwin D. Gibson in using the laboratory facilities associated with them is appreciated. The author wishes to express his sincere thanks to Dr Albert J. Bevolo for the Auger spectroscopic analysis of Specimen 13. The technical assistance of Mr Lester K. Reed and Mr Harlan H. Baker without which this work could not have been carried out is gratefully acknowledged. Also, the help of scientific and technical staff of the Materials Preparation Centre, in particular, of Mr Frederick A. Schmidt, John T. Wheelock, Lanny P. Lincoln and Marv E. Thompson in preparing the alloys in the required form is very much appreciated. This work was performed for the United States Department of Energy, Office of Basic Energy Sciences, Division of Materials Sciences, under contract number: W-7405-Eng-82. This manuscript was presented at the Symposium on Refractory Metals at the AIME Fall Meeting of 1984, Detroit, Michigan.

References

1. T. E. TIETZ and J. W. WILSON, "Behaviour and Properties of Refractory Metals", (Stanford University Press, Stanford, 1965) p. 121.
2. H. R. BABITZE, G. ASAI and H. KATO, "High temperature refractory metals and alloys", Metals Society Conferences, Gordon and Breach, New York, 1964.
3. W. ROSTOKER, "The Metallurgy of vanadium" (Wiley Interscience, New York, 1958) p. 83.
4. H. A. WILHELM, O. N. CARLSON and J. M. DICKINSON, *J. Met., Trans. AIME* **200** (1954) 915.
5. A. L. EUSTICE and O. N. CARLSON, *Trans. ASM.* **53** (1961) 501.
6. C. J. McHARGUE, *Trans. TMS-AIME.* **224** (1962) 334.
7. J. O. STIEGLER and C. J. McHARGUE, in "Deformation Twinning", Edited by R. E. Reed-Hill, J. P. Hirth and H. C. Rogers (Gordon and Breach, New York, 1963).
8. C. J. McHARGUE and H. E. COY, *Trans. TMS-AIME.* **227** (1963) 1170.
9. D. O. HOBSON, J. O. STIEGLER and C. J. McHARGUE, *ibid.* **233** (1965) 1138.
10. C. V. OWEN, D. -S. CHEONG, O. BUCK and T. E. SCOTT, *Met. Trans.* **15A** (1984) 147.
11. T. E. MITCHELL, R. A. FOXALL and P. B. HIRSCH, *Phil. Mag.* **8** (1963) 1895.
12. C. N. REID, A. GILBERT and G. T. HAHN, *Acta Met.* **14** (1966) 975.
13. D. K. BOWEN, J. W. CHRISTIAN and G. TAYLOR, *Can. J. Phys.* **45** (1967) 903.
14. R. A. FOXALL, M. S. DUESBERRY and P. B. HIRSCH, *ibid.* **45** (1967) 607.
15. M. S. DUESBERRY and R. A. FOXALL, *Phil. Mag.* **20** (1969) 719.
16. F. LOUCHET and L. P. KUBIN, *Acta Met.* **23** (1975) 17.
17. C. D. STATHAM and J. W. CHRISTIAN, *Scripta Met.* **5** (1971) 399.
18. J. W. CHRISTIAN, *Met. Trans.* **14A** (1983) 1237.
19. G. TAYLOR and J. W. CHRISTIAN, *Phil. Mag.* **15** (1967) 873; *ibid.* **15** (1967) 893.
20. K. RAVI and R. GIBALA, *Met. Trans.* **2** (1971) 1219.
21. S. GAHR, M. L. GROSSBECK and H. K. BIRNBAUM, *Acta Met.* **25** (1977) 125.
22. S. GAHR and H. K. BIRNBAUM, *Acta Met.* **26** (1978) 1781.
23. M. L. GROSSBECK and H. K. BIRNBAUM, *ibid.* **25** (1977) 135.
24. J. K. TIEN, A. W. THOMPSON, I. M. BERNSTEIN and R. J. RICHARDS, *Met. Trans.* **12A** (1981) 835.
25. L. P. KUBIN, in "Hardening of Metals", Edited by P. Feltham, (Trans. Tech. SA, 1980) ch. 3, p. 67.
26. C. V. OWEN, Private communication, 1984.
27. C. N. REID, *Met. Trans.* **12A** (1981) 371.
28. R. HULTGREN, R. L. OHR and K. KELLY, "Supplement to selected values of thermodynamic properties of metals and alloys", (American Society of Metals, Metals Park, Ohio, 1973).
29. F. A. SCHMIDT, Private communication, 1984.
30. C. N. REID, "Deformation Geometry for Materials Scientists", (Pergamon Press, New York, 1973) ch. 7, p. 183.
31. B. D. CULLITY, "X-ray Diffraction", (Addison-Wesley, 1967) p. 251.
32. R. H. RICHMAN, in "Deformation Twinning", Edited by R. E. Reed-Hill, J. P. Hirth and H. C. Rogers (Gordon and Breach, New York, 1963).
33. A. W. SLEESWYK, *Acta Met.* **10** (1962) 705.
34. S. MAHAJAN, *J. Phys. F., Met. Phys.* **2** (1972) 19.
35. *Idem, Met. Trans.* **12A** (1981) 379.
36. *Idem,* "Mechanical Properties of bcc metals", edited by M. Meshii, (The Metallurgical Society of AIME, Warrendale, Pennsylvania, (1981) p. 225.
37. E. OROWAN, *Proc. Int. Conf. Phys.* (The Physical Society, London) **2** (1934) 81.
38. E. D. HONDROS and D. McLEAN, *Phil. Mag.* **29** (1974) 771.
39. E. D. HONDROS and M. P. SEAH, *Int. Met. Review.* **22** (1977) 262.
40. H. G. F. WISDORF, *Mater. Sci. Engng.* **59** (1983) 1.
41. A. H. COTTRELL, *Trans. AIME.* **212** (1958) 192.
42. A. N. STROH, *Advan. in Physics* **6** (1957) 418.
43. D. HULL, "Fracture of Solids", Proceedings of the International Conference, August 1962, Maple Valley, Washington (John Wiley and Sons, 1962) p. 417.
44. M. J. MARCINKOWSKI and H. J. LEAMY, *J. Appl. Phys.* **40** (1969) 3095.
45. K. JAGANNADHAM and M. J. MARCINKOWSKI, "Unified Theory of Fracture", (Trans. Tech, SA, 1983).
46. R. A. SACK, *Proc. Phys. Soc. (London)* **58** (1946) 729.
47. R. W. ARMSTRONG and P. J. WORTHINGTON, "Metallurgical effects at high strain rates", Edited by R. W. Rohde, B. M. Butcher, J. R. Holland and C. H. Harnes (Plenum, New York, 1973).
48. N. A. BOUCHER and J. W. CHRISTIAN, *Acta Met.* **20** (1972) 581.
49. V. VITEK and J. W. CHRISTIAN, 13th International Conference on the Strength of Metals and Alloys, Cambridge, (Institute of Metals, London, 1973) p. 534.
50. J. F. MILLER and D. C. WESTLAKE, *Trans. Jpn. Inst. Metals,* **21** (1980) 153.
51. M. J. MARCINKOWSKI, M. E. TAYLOR and F. X. KAYSER, *J. Mater. Sci.* **10** (1975) 406.
52. J. H. WESTBROOK, *Met. Rev.* **9** (1965) 415.

Received 11 August 1986
and accepted 11 February 1987